Volume 7
Number 6
21 March 2025
Pages 1477–1756

Nanoscale Advances

rsc.li/nanoscale-advances

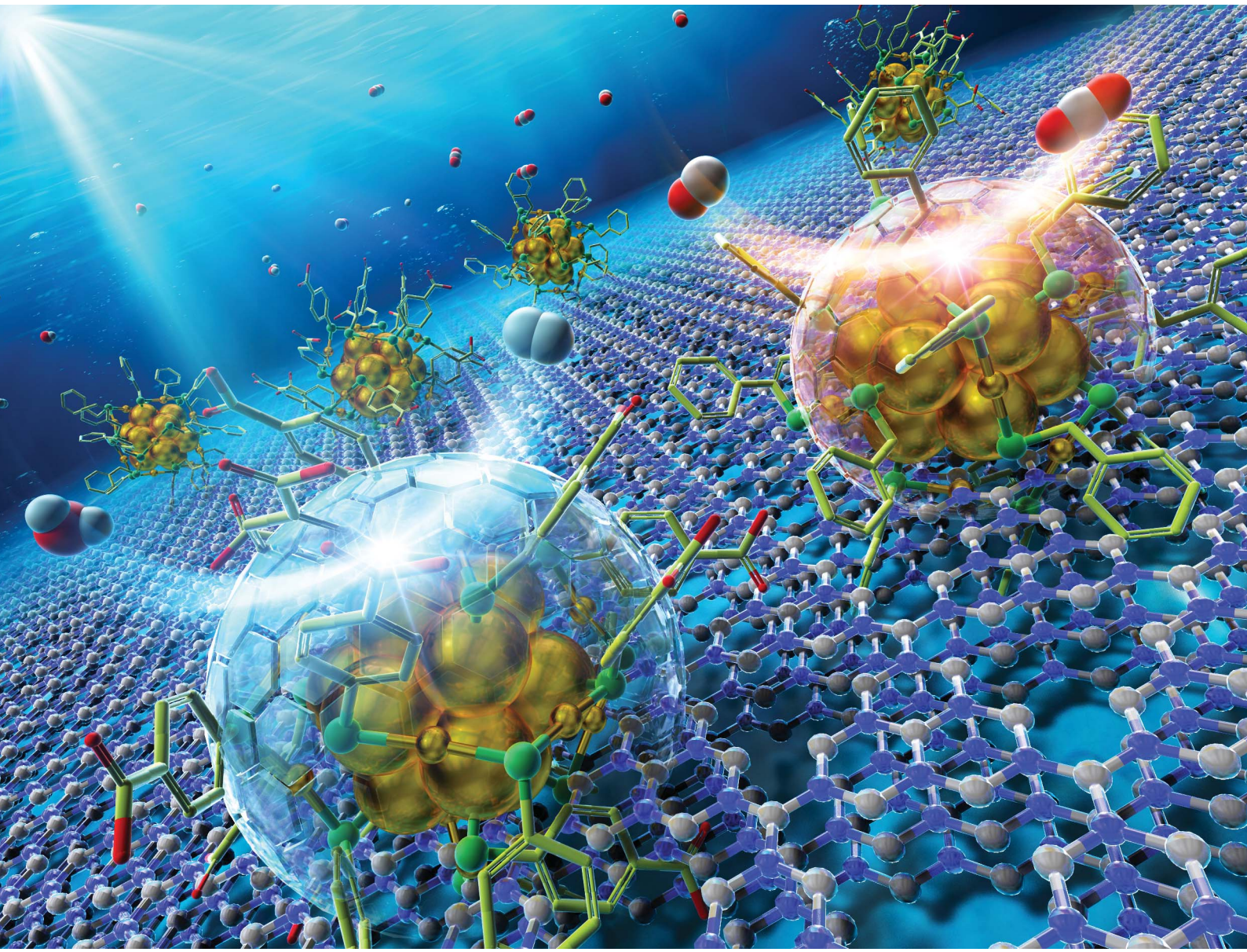

ISSN 2516-0230

ROYAL SOCIETY OF CHEMISTRY

PAPER

Tokuhisa Kawawaki, Yuichi Negishi *et al.*
Activation of photocatalytic CO_2 reduction by loading hydrophobic thiolate-protected Au_{25} nanocluster cocatalyst

NCNST

Nanoscale Advances

ROYAL SOCIETY OF CHEMISTRY

PAPER

View Article Online
View Journal | View Issue

Check for updates

Cite this: *Nanoscale Adv.*, 2025, **7**, 1518

Activation of photocatalytic CO_2 reduction by loading hydrophobic thiolate-protected Au_{25} nanocluster cocatalyst†

Yuki Yamazaki,‡[a] Yuki Tomoyasu,‡[a] Tokuhisa Kawawaki *[ab] and Yuichi Negishi *[bc]

Received 18th December 2024
Accepted 11th February 2025

DOI: 10.1039/d4na01045k

rsc.li/nanoscale-advances

The photocatalytic carbon dioxide (CO_2) reduction reaction (CO_2RR), which reduces CO_2 to various useful chemical compounds by light, has attracted attention to achieve carbon neutrality. In photocatalytic CO_2RR, it is effective to load metal nanoparticles (NP) as cocatalysts on the surface of semiconductor photocatalysts to improve their activity and selectivity. In this study, we used ultrafine metal nanoclusters (NC) with a particle size of about 1 nm as cocatalysts to clarify the effect of surface ligands on the activity and selectivity of the photocatalytic CO_2RR. As a result, it was shown that the introduction of hydrophobic ligands to the Au_{25} NC cocatalyst suppresses the competing hydrogen evolution reaction, thereby increasing the selectivity of CO_2RR. In addition, the hydrophobic ligand-protected Au_{25} NC cocatalysts exhibited 66 times higher CO evolution rates per Au-loading weights than the Au NP cocatalysts with a particle size of about 7 nm. These results provide crucial insights into the creation of highly active metal NC cocatalysts for photocatalytic CO_2RR.

Open Access Article. Published on 12 February 2025. Downloaded on 2/7/2026 9:34:12 AM.
This article is licensed under a Creative Commons Attribution 3.0 Unported Licence.

Introduction

The photocatalytic carbon dioxide (CO_2) reduction reaction (CO_2RR), which reduces CO_2 by light, is expected to be put to practical use as one of the means to solve energy, environmental and resource issues.[1,2] This is because if exceedingly stable CO_2 can be converted into various useful chemical compounds using sunlight, CO_2 can be recycled and we can break free from the conventional energy systems that rely on fossil resources. For the practical use of the photocatalytic CO_2RR, it is essential to further improve the efficiency and selectivity of the reduction products. Herein, commonly used photocatalysts are composed of a semiconductor photocatalyst and a metal/metal oxide cocatalyst. Importantly, many semiconductor photocatalysts that have a band gap suitable for CO_2RR have been developed, and visible-light-driven photocatalysts that can respond to visible light rather than only ultraviolet light have been actively investigated in recent years.[3–7] At the same time, the selection/fabrication of appropriate cocatalyst nanoparticles (NP) that have a significant impact on their activity and selectivity have also been developed. For example, it has been reported that Ag and Au NP cocatalysts mainly produce CO,[8–13] whereas Pd, Cu and Rh–Ru alloy NP cocatalysts mainly produce CH_4.[2,14–17]

In addition, it is known that using smaller cocatalysts improves the activity of the catalytic reaction. In particular, when metal nanoclusters[18–25] (NC) with a particle size of about 1 nm are used as cocatalysts, their photocatalytic activity for water splitting is greatly improved.[26–32] This improvement is mainly due to (1) the increase in the number of active sites due to the increase in the specific surface area and (2) the optimization of the adsorption characteristics with the reaction substrates due to the change in the electronic state based on the quantum size effect. In general, the water splitting activity of metal NC cocatalysts for photocatalysts is improved when (i) their surfaces are protected by ligands with hydrophilic functional groups[33] or (ii) the hydrophobic ligands are removed.[28,34] This is because the presence of hydrophilic functional groups or removal of hydrophobic ligands makes it easier to be approached by protons (H^+), which are the reaction substrate, on the surface metal atoms of the metal NC. By contrast, in photocatalytic CO_2RR, the hydrogen evolution reaction (HER) due to water splitting is a competitive reaction. Therefore, if such photocatalytic HER can be suppressed by enhancing the hydrophobicity of the surface ligands, high selectivity and activity for photocatalytic CO_2RR is expected to be obtained (Fig. 1A).

[a]*Department of Applied Chemistry, Faculty of Science, Tokyo University of Science, 1-3 Kagurazaka, Shinjuku-ku, Tokyo 162-8601, Japan*

[b]*Carbon Value Research Center, Research Institute for Science & Technology, Tokyo University of Science, 2641 Yamazaki, Noda, Chiba 278-8510, Japan*

[c]*Institute of Multidisciplinary Research for Advanced Materials, Tohoku University, Katahira 2-1-1, Aobaku, Sendai 980-8577, Japan*

† Electronic supplementary information (ESI) available: Experiment, characterization, additional figures, characterization of Au NC, additional UV-vis, XANES, FT-EXAFS, EXAFS spectra, TEM image and photocatalytic activity. See DOI: https://doi.org/10.1039/d4na01045k

‡ These authors contributed equally to this work.

© 2025 The Author(s). Published by the Royal Society of Chemistry

Open Access Article. Published on 12 February 2025. Downloaded on 2/7/2026 9:34:12 AM.
This article is licensed under a Creative Commons Attribution 3.0 Unported Licence.

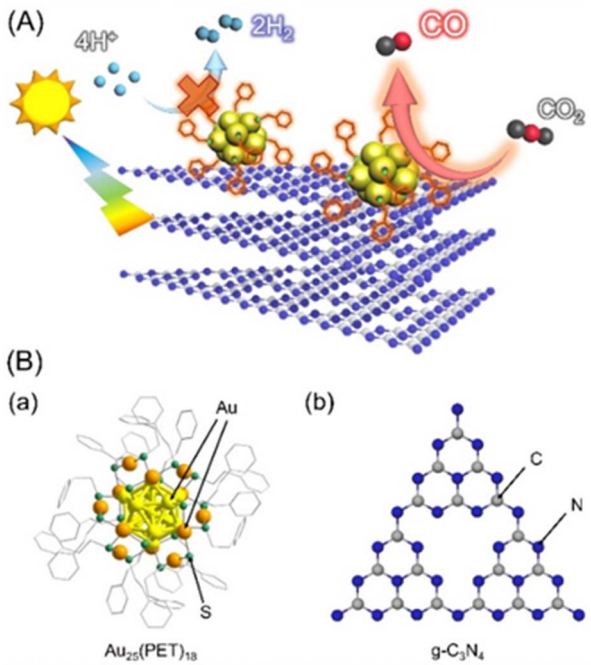

Fig. 1 (A) Schematic of the purposes of this study and (B) geometric structure of (a) $Au_{25}(PET)_{18}$ and (b) gCN photocatalysts.

In this study, we attempted to experimentally verify such an assumption regarding the effects of the functionality of ligands of metal NC on photocatalytic CO_2RR activity. Specifically, we used Au_{25} NC[35,36] (Fig. 1B(a)), which are the most common model NC with high electrocatalytic CO_2RR activity[37–40] as cocatalysts and attempted to clarify the effects of hydrophobic and hydrophilic ligands that protect them during photocatalytic CO_2RR activity. As a result, it was shown that the introduction of hydrophobic ligand-protected Au_{25} NC cocatalyst suppressed the competing HER, thereby increasing the selectivity of the CO_2RR and it exhibited 66 times higher CO evolution rates per Au-loading weight than the Au NP cocatalysts made by a conventional photodeposition (PD) method.

Results and discussion

In this study, we used g-C_3N_4 photocatalysts (gCN; Fig. 1B(b)), which have attracted much attention as a next-generation visible-light-driven photocatalyst because of their ease of synthesis, nontoxic nature, abundant availability of the raw materials on the Earth, and high physical and chemical stability.[41–45] There have also been many reports of gCN as a photocatalyst for photocatalytic CO_2RR.[46–48] We synthesized gCN from urea by thermal polymerization as previously reported,[29] and measured the powder X-ray diffraction and diffuse reflectance (DR) spectrum of the obtained gCN. From these results, we confirmed that the synthesized photocatalyst was visible-light-responsive g-C_3N_4 with relatively high crystallinity (Fig. S1†).

Next, Au_{25} NC protected by 2-phenylethanethiolate (PET), a hydrophobic ligand, was synthesized by a previously reported method ($Au_{25}(PET)_{18}$; Fig. S2 and S3†).[27,49] The obtained $Au_{25}(PET)_{18}$ was dissolved in acetone and loaded on gCN using an impregnation method ($Au_{25}(PET)_{18}$/gCN). We characterized the prepared $Au_{25}(PET)_{18}$/gCN using various methods (Fig. 2 and S4†). The transmission electron microscopy (TEM) image of $Au_{25}(PET)_{18}$/gCN shown in Fig. 2a showed that the particle size of $Au_{25}(PET)_{18}$ cocatalysts on gCN (particle size: 1.11 ± 0.19 nm) was almost the same as $Au_{25}(PET)_{18}$ before adsorption on gCN (particle size: 1.03 ± 0.13 nm). Compared with the sizes of the Au NP cocatalysts of Au NP-loaded gCN (Au NP/gCN; particle size: 6.55 ± 1.35 nm; Fig. 2c and S5†) prepared using the conventional PD method, $Au_{25}(PET)_{18}$ cocatalysts have smaller and monodispersed sizes. The Au L_3-edge X-ray absorption near edge structure (XANES) spectra showed that (1) the $Au_{25}(PET)_{18}$ cocatalyst on gCN has a metallic electronic state and (2) the electronic state of $Au_{25}(PET)_{18}$ is maintained before and after adsorption on gCN (Fig. 3A and S4†). Such the change in the electronic state between the Au cocatalyst and gCN was not observed by XPS (Fig. S6†). The Au L_3-edge Fourier transform

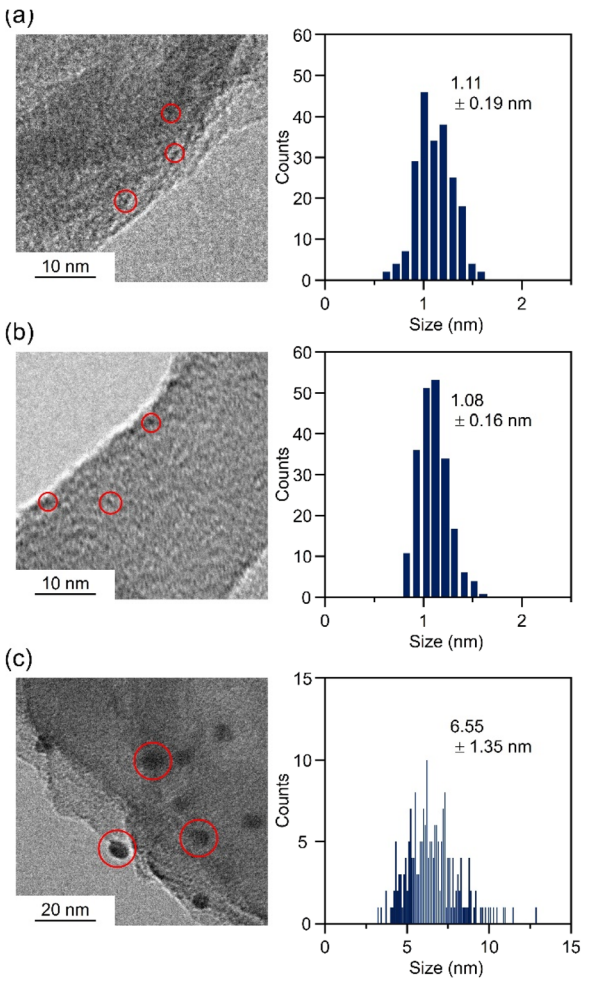

Fig. 2 TEM images and resulting histograms of the particle-size distribution for Au cocatalysts for (a) $Au_{25}(PET)_{18}$/gCN, (b) Au_{25}(PET, *p*-MBA)$_{18}$/gCN and (c) Au NP/gCN. Loading amounts of Au are 0.1, 0.1 and 3.0 wt% for $Au_{25}(PET)_{18}$/gCN, Au_{25}(PET, *p*-MBA)$_{18}$/gCN and Au NP/gCN, respectively.

Open Access Article. Published on 12 February 2025. Downloaded on 2/7/2026 9:34:12 AM.
This article is licensed under a Creative Commons Attribution 3.0 Unported Licence.

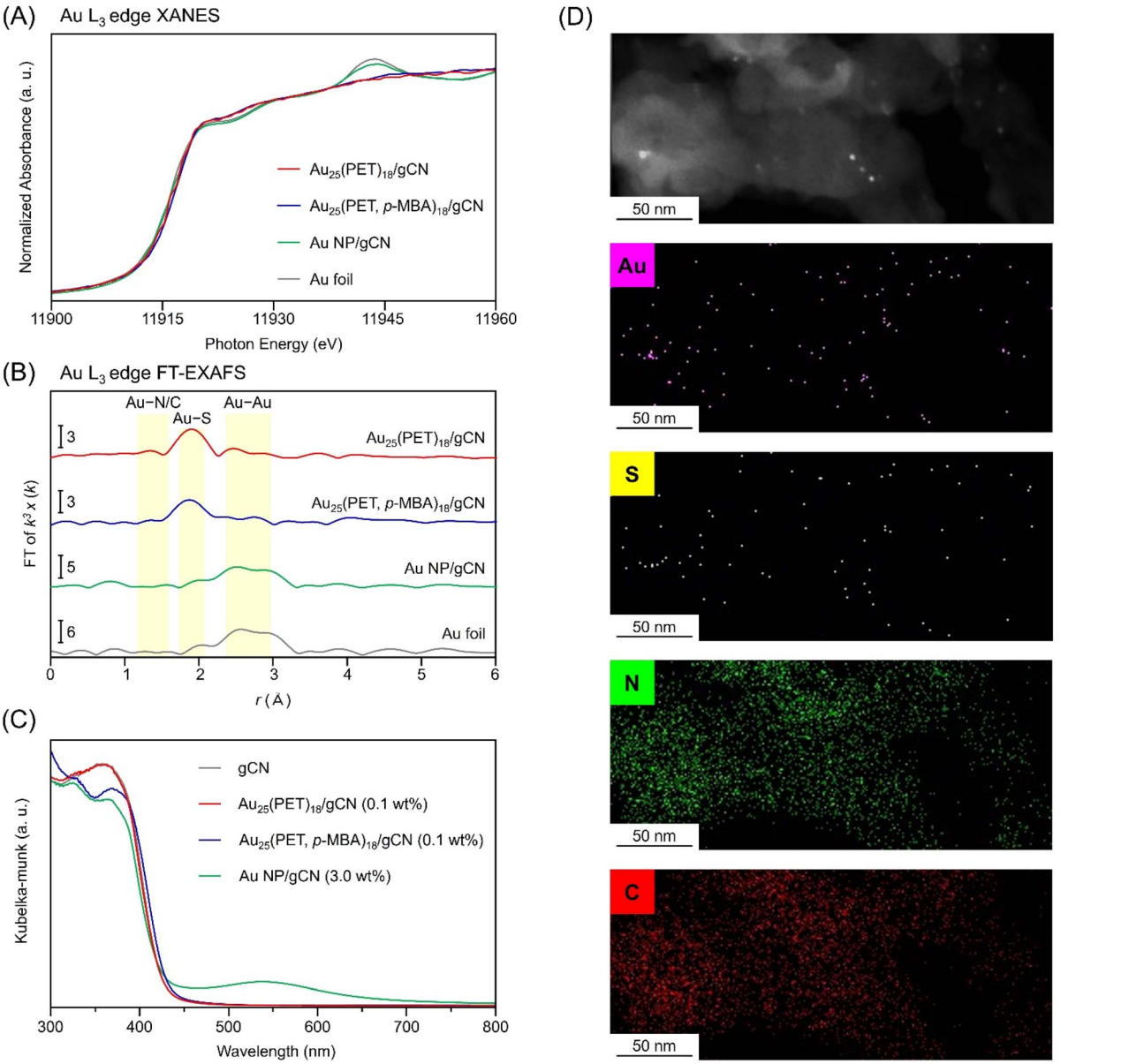

Fig. 3 Characterization of cocatalyst-loaded gCN photocatalysts. Au L_3-edge (A) XANES, (B) FT-EXAFS spectra and (C) DR spectra. (D) HAADF–STEM images and EDS elemental mapping of $Au_{25}(PET)_{18}$/gCN (Au–M, S–K, C–K and N–K). In (A and B), Au L_3-edge XANES and FT-EXAFS spectra of Au foil is also shown for comparison. In (B), the peaks at ≈1.9 and 2.6–3.0 Å are assigned to the Au–S and Au–Au bonds, respectively. Loading amounts of Au are 0.1, 0.1 and 3.0 wt% for $Au_{25}(PET)_{18}$/gCN, Au_{25}(PET, *p*-MBA)$_{18}$/gCN and Au NP/gCN, respectively.

extended X-ray absorption fine structure (FT-EXAFS) spectra showed a peak (≈1.9 Å) due to the Au–S bond, suggesting that the SR ligands of $Au_{25}(PET)_{18}$ remain even after adsorption and that their geometric structure is mostly maintained (Fig. 3B and S4†). In the DR spectrum, there is no strong absorption in the visible region due to localized surface plasmon resonance, as seen in Au NP formed by aggregation (Fig. 3C and S4†). In an energy dispersive X-ray spectroscopy (EDS) elemental mapping obtained using a high-angle annular dark field–scanning TEM (HAADF–STEM) (Fig. 3D), Au and S were mapped to the same location, confirming that $Au_{25}(PET)_{18}$ cocatalyst was located on gCN. These analyses strongly indicated that $Au_{25}(PET)_{18}$ cocatalyst was loaded on gCN while largely maintaining its geometric structure.

The photocatalytic CO_2RR activity of the $Au_{25}(PET)_{18}$/gCN was evaluated using a reaction cell under CO_2 flow with light irradiation (Fig. 4). In the measurement, triisopropanolamine (TIPA) was added (20 vol%) as a hole sacrificial reagent to correctly evaluate the photocatalytic CO_2RR activity.[50] The Au cocatalyst-loaded gCN was dispersed in water with the sacrificial agent, it was irradiated with visible light using a blue LED (405 nm), and H_2 or CO evolution was quantified using a gas chromatograph at regular time intervals (Fig. S7†). By analysing the reaction solution with a high-performance liquid

© 2025 The Author(s). Published by the Royal Society of Chemistry

Open Access Article. Published on 12 February 2025. Downloaded on 2/7/2026 9:34:12 AM.
This article is licensed under a Creative Commons Attribution 3.0 Unported Licence.

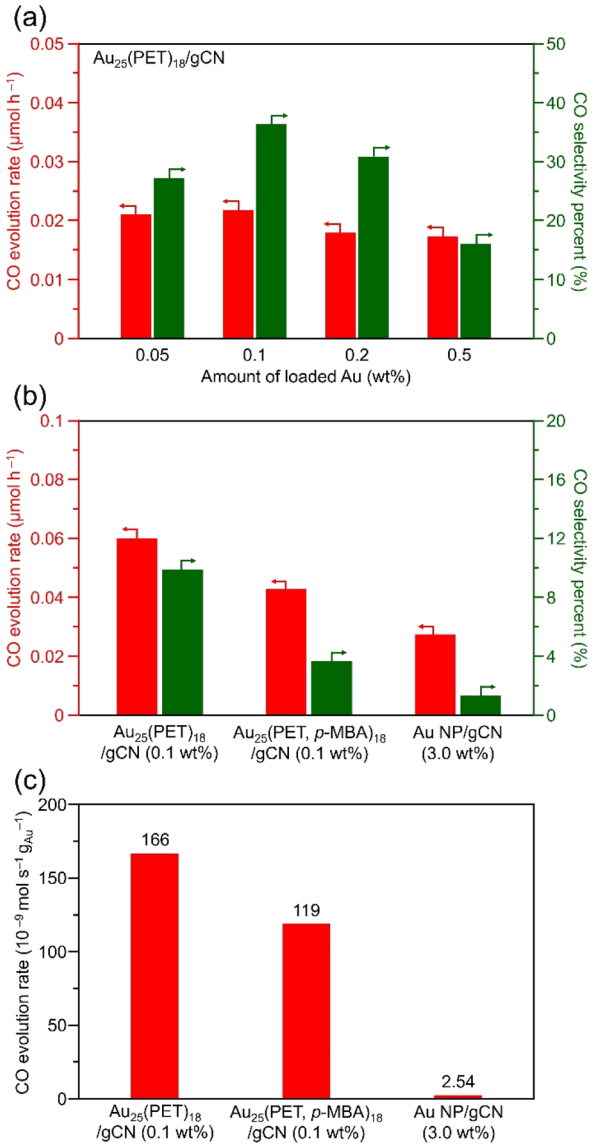

Fig. 4 Photocatalytic CO_2RR activity of Au cocatalyst-loaded gCN photocatalysts. (a) Dependence on loading weight of Au for $Au_{25}(PET)_{18}$/gCN. (b) Comparisons of CO evolution rates and resulting CO selectivities and (c) CO evolution rates per loading weight of Au, for $Au_{25}(PET)_{18}$/gCN, $Au_{25}(PET, p\text{-}MBA)_{18}$/gCN and Au NP/gCN. Photocatalyst: 100 mg, solution: water (60 mL) with TIPA (12.5 g), flow gas: CO_2 (1 atm), light source: 405 nm LED lamp and cell: top-irradiation cell. In (b) and (c), loading weights of Au are 0.1, 0.1 and 3.0 wt% for $Au_{25}(PET)_{18}$/gCN, $Au_{25}(PET, p\text{-}MBA)_{18}$/gCN and Au NP/gCN, respectively.

chromatograph, it was confirmed that the product did not contain any liquid-phase CO_2RR products. In addition, by evaluating the same measurement under Ar flow, it was confirmed that the obtained CO was derived from the flowing CO_2 (Fig. S8†).

For the photocatalytic CO_2RR experiments, we first investigated the optimal Au-loading weights of $Au_{25}(PET)_{18}$/gCN. As a result, the highest CO evolution rate was obtained when the Au-loading weight was set to 0.1 wt% (Fig. 4a). Therefore, in the subsequent experiments, we used $Au_{25}(PET)_{18}$/gCN prepared with this optimal 0.1 wt% of Au-loading weight.

Next, we investigated the effects of hydrophilic and hydrophobic ligands on Au_{25} NC on the photocatalytic CO_2RR activity. In our previous report, we have succeeded in improving the hydrophilicity of Au_{25} NC by exchanging some of the ligands of $Au_{25}(PET)_{18}$ with 4-mercaptobenzoic acid (*p*-MBA), a hydrophilic ligand with a structure relatively similar to that of PET.[27] Accordingly, we prepared Au_{25} NC in which some of the ligands were exchanged by *p*-MBA ($Au_{25}(PET, p\text{-}MBA)_{18}$; Fig. S2 and S3†), and loaded it on gCN by a liquid-phase adsorption method to prepare a photocatalyst ($Au_{25}(PET, p\text{-}MBA)_{18}$/gCN; Fig. 2b, 3 and S9†). The photocatalytic CO_2RR activity of the obtained $Au_{25}(PET, p\text{-}MBA)_{18}$/gCN is shown in Fig. 4b. Interestingly, it was found that hydrophilic $Au_{25}(PET, p\text{-}MBA)_{18}$/gCN has 2.70 times lower CO selectivity ($selectivity_{CO}$ = 3.66%) than hydrophobic $Au_{25}(PET)_{18}$/gCN ($selectivity_{CO}$ = 9.87%). Jiang and Lee *et al.* reported that $Au_{25}(SR)_{18}$ protected by a hydrophilic ligand (3-mercaptopropanoic acid or 3-mercapto-1-propanesulfonic acid), which allowed efficient H^+ relay, had a higher electrochemical HER than hydrophobic 1-hexanethiolate (SC_6) ligand-protected $Au_{25}(SC_6)_{18}$.[33] In our study, the photocatalytic HER selectivity was also improved when hydrophilic $Au_{25}(PET, p\text{-}MBA)_{18}$/gCN was used, probably because *p*-MBA induced an effective H^+ relay. Although hydrophilic NC were used as cocatalysts in photocatalytic CO_2RR in the previous report,[51] this study demonstrated that the use of these hydrophilic NC as cocatalysts (1) promoted the HER as a competing reaction and (2) thereby reduced the selectivity of the CO_2RR (Fig. 4b and c).

Next, we compared the photocatalytic CO_2RR activity between $Au_{25}(PET)_{18}$/gCN, which has a hydrophobic ligand suitable for photocatalytic CO_2RR, and Au NP/gCN prepared using a conventional PD method (Fig. 4b). In this experiment, we also optimized the Au-loading weights of Au NP/gCN, which was found to be 3.0 wt% of Au (Fig. S10 and S11†). The results of the comparison for their photocatalytic CO_2RR activity are also shown in Fig. 4b. The results demonstrated that (1) even though the Au-loading weight of $Au_{25}(PET)_{18}$/gCN was 30 times less than that of Au NP/gCN, $Au_{25}(PET)_{18}$/gCN shows higher CO evolution rate than Au NP/gCN (0.06 *vs.* 0.03 $\mu mol_{CO}\ h^{-1}$, Fig. 4b) and (2) $Au_{25}(PET)_{18}$/gCN shows a greatly suppressed H_2 evolution rate compared with Au NP/gCN (0.61 *vs.* 2.10 $\mu mol_{H2}\ h^{-1}$, Fig. 4b). Comparing the CO evolution rate per Au-loading weight in Fig. 4c, $Au_{25}(PET)_{18}$/gCN and $Au_{25}(PET, p\text{-}MBA)_{18}$/gCN showed 66 and 47 times higher CO evolution rates than Au NP/gCN, respectively (166 *vs.* 119 *vs.* 2.54×10^{-9} mol s^{-1} $g_{Au}{}^{-1}$). Accordingly, $Au_{25}(PET)_{18}$/gCN showed the highest CO selectivity (9.87% *vs.* 3.66% *vs.* 1.31% for $Au_{25}(PET)_{18}$/gCN, $Au_{25}(PET, p\text{-}MBA)_{18}$ and Au NP/gCN, respectively). The previous study[38] reported that $Au_{25}(SR)_{18}$ has a suitable CO_2 adsorption site. Furthermore, molecular dynamics simulations suggested that the presence of hydrophilic ligands in $[Au_{25}(SR)_{18}]^-$ efficiently induced HER due to enhanced proton transfer facilitated by hydrogen bonds.[52] Therefore, it can be considered that $Au_{25}(PET)_{18}$/gCN promoted photocatalytic CO_2RR with a relatively high CO selectivity because $Au_{25}(PET)_{18}$/gCN contains

© 2025 The Author(s). Published by the Royal Society of Chemistry

Open Access Article. Published on 12 February 2025. Downloaded on 2/7/2026 9:34:12 AM.
This article is licensed under a Creative Commons Attribution 3.0 Unported Licence.

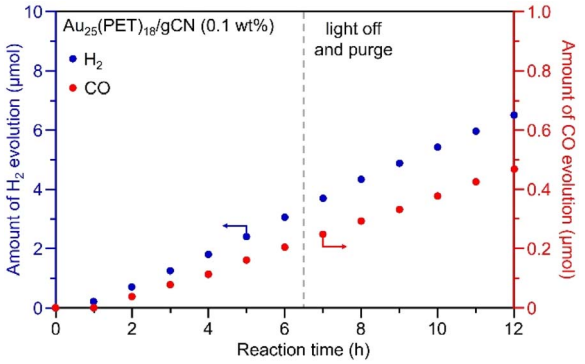

Fig. 5 Time dependence of photocatalytic CO_2RR activity of $Au_{25}(PET)_{18}$/gCN. Photocatalyst: 100 mg, solution: water (60 mL) with TIPA (12.5 g), flow gas: CO_2 (1 atm), light source: 405 nm LED lamp and cell: top-irradiation cell. Loading weight of Au is 0.1 wt% for $Au_{25}(PET)_{18}$/gCN.

both the suitable CO_2 adsorption site and hydrophobic PET which leads to the suppression of HER.

Finally, we evaluated the catalytic stability of $Au_{25}(PET)_{18}$/gCN, which has a relatively good CO evolution rate and selectivity. In general, the excited electrons generated by the photocatalytic reaction have a strong reduction power and may reductively decompose many organic substances. Therefore, we measured the long-term photocatalytic CO_2RR activity of $Au_{25}(PET)_{18}$/gCN to evaluate its durability. As a result, it was shown that $Au_{25}(PET)_{18}$/gCN stably produced CO and its selectivity did not change even after 12 h of visible-light irradiation (Fig. 5). We also investigated the size of the cocatalyst after the photocatalytic activity test using TEM. As a result, the particle size of the $Au_{25}(PET)_{18}$ cocatalyst was almost the same as that of the $Au_{25}(PET)_{18}$ just after loading on gCN (particle size: 1.11 ± 0.17 nm; Fig. S4A†). In fact, no change in the diffraction pattern due to Au aggregation was observed in the powder X-ray diffraction (Fig. S12†). Au L_3-edge XANES spectra showed that the electronic state of the $Au_{25}(PET)_{18}$ cocatalyst did not change significantly before and after light irradiation (Fig. S4C†). Furthermore, surprisingly, the peak (≈1.9 Å) derived from the Au–S bond was maintained in the Au L_3-edge FT-EXAFS spectrum even after the evaluation of photocatalytic CO_2RR activity (Fig. S4D†), suggesting that most of the ligands remain undecomposed even after long-term light irradiation. These results revealed that $Au_{25}(PET)_{18}$/gCN, which has a strong Au–S bond, has high stability against light irradiation.

Conclusions

The loading of metal NC cocatalysts leads to a significant improvement in photocatalytic activity. In this study, we investigated the effect of organic ligands protecting the surface of these metal NC cocatalysts on the activity and selectivity of photocatalytic CO_2RR. The results demonstrated that (1) the introduction of hydrophilic ligands to the Au_{25} NC cocatalyst promotes the competing HER, whereas (2) the introduction of hydrophobic ligands to the Au_{25} NC cocatalyst suppresses the HER, leading to the progress of photocatalytic CO_2RR with relatively high CO selectivity. In this way, although it has been generally believed that the presence of organic ligands on the metal NC surface reduces photocatalytic activity, this study revealed that the presence of hydrophobic ligands effectively suppresses the competing HER in photocatalytic CO_2RR. Furthermore, it was found that the hydrophobic $Au_{25}(PET)_{18}$-loaded photocatalysts show a 66 times higher CO evolution rate per Au-loading weight and relatively high CO selectivity compared with Au NP-loaded photocatalysts. These results will provide clear design guidelines for achieving high-performance photocatalytic CO_2RR by loading metal NC cocatalysts. In the future, it is expected that the obtained knowledge will be applied to a semiconductor photocatalyst suitable for photocatalytic CO_2RR[17] to create high-performance CO_2RR photocatalysts with significantly improved selectivity and activity, which will contribute to practical use (Fig. S13†).

Data availability

All data generated in this study are provided in the manuscript and ESI.†

Author contributions

T. K. and Y. N. conceived the research and designed the experiments. Y. Y., Y. T., and T. K. performed the syntheses, characterization and measurements of the CO_2RR activity. T. K. and Y. N. wrote the manuscript.

Conflicts of interest

There are no conflicts to declare.

Acknowledgements

The authors thank Mr Kengo Nagatsuka, Dr Yuichi Yamaguchi and Prof. Akihiko Kudo (Tokyo University of Science) for technical assistance. This work was supported by the Japan Society for the Promotion of Science (JSPS) KAKENHI (grant numbers 23H00289, 22K19012 and 24K01459). Funding from the Carbon Recycling Fund Institute, the Japan Gas Association, the Iwatani Naoji Foundation, the Ichimura Foundation for New Technology, the Suzuki Foundation, and the Japan Keirin Autorace Foundation is gratefully acknowledged.

Notes and references

1 J. L. White, M. F. Baruch, J. E. Pander III, Y. Hu, I. C. Fortmeyer, J. E. Park, T. Zhang, K. Liao, J. Gu, Y. Yan, T. W. Shaw, E. Abelev and A. B. Bocarsly, *Chem. Rev.*, 2015, **115**, 12888–12935.
2 X. Li, J. Yu, M. Jaroniec and X. Chen, *Chem. Rev.*, 2019, **119**, 3962–4179.
3 A. Kudo and Y. Miseki, *Chem. Soc. Rev.*, 2009, **38**, 253–278.
4 B. A. Pinaud, J. D. Benck, L. C. Seitz, A. J. Forman, Z. Chen, T. G. Deutsch, B. D. James, K. N. Baum, G. N. Baum,

© 2025 The Author(s). Published by the Royal Society of Chemistry

Open Access Article. Published on 12 February 2025. Downloaded on 2/7/2026 9:34:12 AM. This article is licensed under a Creative Commons Attribution 3.0 Unported Licence.

S. Ardo, H. Wang, E. Miller and T. F. Jaramillo, *Energy Environ. Sci.*, 2013, **6**, 1983–2002.
5 Y. Wang, H. Suzuki, J. Xie, O. Tomita, D. J. Martin, M. Higashi, D. Kong, R. Abe and J. Tang, *Chem. Rev.*, 2018, **118**, 5201–5241.
6 D. M. Fabian, S. Hu, N. Singh, F. A. Houle, T. Hisatomi, K. Domen, F. E. Osterloh and S. Ardo, *Energy Environ. Sci.*, 2015, **8**, 2825–2850.
7 Q. Wang and K. Domen, *Chem. Rev.*, 2020, **120**, 919–985.
8 K. Iizuka, T. Wato, Y. Miseki, K. Saito and A. Kudo, *J. Am. Chem. Soc.*, 2011, **133**, 20863–20868.
9 K. Teramura, Z. Wang, S. Hosokawa, Y. Sakata and T. Tanaka, *Chem.–Eur. J.*, 2014, **20**, 9906–9909.
10 K. Teramura and T. Tanaka, *Phys. Chem. Chem. Phys.*, 2018, **20**, 8423–8431.
11 S. Yoshino, T. Takayama, Y. Yamaguchi, A. Iwase and A. Kudo, *Acc. Chem. Res.*, 2022, **55**, 966–977.
12 M. Yamamoto, T. Yoshida, N. Yamamoto, T. Nomoto, Y. Yamamoto, S. Yagi and H. Yoshida, *J. Mater. Chem. A*, 2015, **3**, 16810–16816.
13 Y. Jiang, Y. Yu, X. Zhang, M. Weinert, X. Song, J. Ai, L. Han and H. Fei, *Angew. Chem., Int. Ed.*, 2021, **60**, 17388–17393.
14 T. Kawawaki, Y. Akinaga, D. Yazaki, H. Kameko, D. Hirayama and Y. Negishi, *Chem.–Eur. J.*, 2023, **29**, e202203387.
15 J. Ran, M. Jaroniec and S.-Z. Qiao, *Adv. Mater.*, 2018, **30**, 1704649.
16 S. N. Habisreutinger, L. Schmidt-Mende and J. K. Stolarczyk, *Angew. Chem., Int. Ed.*, 2013, **52**, 7372–7408.
17 W. Soontornchaiyakul, S. Yoshino, T. Kanazawa, R. Haruki, D. Fan, S. Nozawa, Y. Yamaguchi and A. Kudo, *J. Am. Chem. Soc.*, 2023, **145**, 20485–20491.
18 Q. Yao, T. Chen, X. Yuan and J. Xie, *Acc. Chem. Res.*, 2018, **51**, 1338–1348.
19 N. A. Sakthivel and A. Dass, *Acc. Chem. Res.*, 2018, **51**, 1774–1783.
20 Z. Gan, N. Xia and Z. Wu, *Acc. Chem. Res.*, 2018, **51**, 2774–2783.
21 A. Ghosh, O. F. Mohammed and O. M. Bakr, *Acc. Chem. Res.*, 2018, **51**, 3094–3103.
22 J. Yan, B. K. Teo and N. Zheng, *Acc. Chem. Res.*, 2018, **51**, 3084–3093.
23 I. Chakraborty and T. Pradeep, *Chem. Rev.*, 2017, **117**, 8208–8271.
24 Y. Du, H. Sheng, D. Astruc and M. Zhu, *Chem. Rev.*, 2020, **120**, 526–622.
25 A. Fernando, K. L. D. M. Weerawardene, N. V. Karimova and C. M. Aikens, *Chem. Rev.*, 2015, **115**, 6112–6216.
26 D. Hirayama, T. Kawawaki, S. Oguchi, M. Ogano, N. Kon, T. Yasuda, A. Higami and Y. Negishi, *J. Am. Chem. Soc.*, 2024, **146**, 26808–26818.
27 T. Kawawaki, Y. Kataoka, M. Hirata, Y. Akinaga, R. Takahata, K. Wakamatsu, Y. Fujiki, M. Kataoka, S. Kikkawa, A. S. Alotabi, S. Hossain, D. J. Osborn, T. Teranishi, G. G. Andersson, G. F. Metha, S. Yamazoe and Y. Negishi, *Angew. Chem., Int. Ed.*, 2021, **60**, 21340–21350.
28 T. Kawawaki, M. Kawachi, D. Yazaki, Y. Akinaga, D. Hirayama and Y. Negishi, *Nanomaterials*, 2022, **12**, 344.
29 D. Yazaki, T. Kawawaki, D. Hirayama, M. Kawachi, K. Kato, S. Oguchi, Y. Yamaguchi, S. Kikkawa, Y. Ueki, S. Hossain, D. J. Osborn, F. Ozaki, S. Tanaka, J. Yoshinobu, G. F. Metha, S. Yamazoe, A. Kudo, A. Yamakata and Y. Negishi, *Small*, 2023, **19**, 2208287.
30 C. M. Pelicano, M. Saruyama, R. Takahata, R. Sato, Y. Kitahama, H. Matsuzaki, T. Yamada, T. Hisatomi, K. Domen and T. Teranishi, *Adv. Funct. Mater.*, 2022, **32**, 2202987.
31 H. Wang, X. Zhang, W. Zhang, M. Zhou and H.-L. Jiang, *Angew. Chem., Int. Ed.*, 2024, **63**, e202401443.
32 A. S. Alotabi, D. J. Osborn, S. Ozaki, Y. Kataoka, Y. Negishi, S. Tesana, G. F. Metha and G. G. Andersson, *Mater. Adv.*, 2022, **3**, 3620–3630.
33 K. Kwak, W. Choi, Q. Tang, D.-e. Jiang and D. Lee, *J. Mater. Chem. A*, 2018, **6**, 19495–19501.
34 Y. Negishi, M. Mizuno, M. Hirayama, M. Omatoi, T. Takayama, A. Iwase and A. Kudo, *Nanoscale*, 2013, **5**, 7188–7192.
35 M. Zhu, C. M. Aikens, F. J. Hollander, G. C. Schatz and R. Jin, *J. Am. Chem. Soc.*, 2008, **130**, 5883–5885.
36 M. W. Heaven, A. Dass, P. S. White, K. M. Holt and R. W. Murray, *J. Am. Chem. Soc.*, 2008, **130**, 3754–3755.
37 T. Kawawaki, T. Okada, D. Hirayama and Y. Negishi, *Green Chem.*, 2024, **26**, 122–163.
38 D. R. Kauffman, D. Alfonso, C. Matranga, H. Qian and R. Jin, *J. Am. Chem. Soc.*, 2012, **134**, 10237–10243.
39 D. R. Kauffman, J. Thakkar, R. Siva, C. Matranga, P. R. Ohodnicki, C. Zeng and R. Jin, *ACS Appl. Mater. Interfaces*, 2015, **7**, 15626–15632.
40 H. Seong, V. Efremov, G. Park, H. Kim, J. S. Yoo and D. Lee, *Angew. Chem., Int. Ed.*, 2021, **60**, 14563–14570.
41 W.-J. Ong, L.-L. Tan, Y. H. Ng, S.-T. Yong and S.-P. Chai, *Chem. Rev.*, 2016, **116**, 7159–7329.
42 Y. Wang, X. Wang and M. Antonietti, *Angew. Chem., Int. Ed.*, 2012, **51**, 68–89.
43 Z. Zhao, Y. Sun and F. Dong, *Nanoscale*, 2015, **7**, 15–37.
44 Y. Zhu, T. Wang, T. Xu, Y. Li and C. Wang, *Appl. Surf. Sci.*, 2019, **464**, 36–42.
45 S. Cao, J. Low, J. Yu and M. Jaroniec, *Adv. Mater.*, 2015, **27**, 2150–2176.
46 Q. Lu, K. Eid, W. Li, A. M. Abdullah, G. Xu and R. S. Varma, *Green Chem.*, 2021, **23**, 5394–5428.
47 J. Lin, W. Tian, H. Zhang, X. Duan, H. Sun and S. Wang, *Energy Fuels*, 2021, **35**, 7–24.
48 Y. Zhou, Z. Wang, L. Huang, S. Zaman, K. Lei, T. Yue, Z. a. Li, B. You and B. Y. Xia, *Adv. Energy Mater.*, 2021, **11**, 2003159.
49 H. Qian, C. Liu and R. Jin, *Sci. China:Chem.*, 2012, **55**, 2359–2365.
50 P. Zhang, T. Sun, L. Xu, Q. Xu, D. Wang, W. Liu, T. Zheng, G. Yang and J. Jiang, *ACS Sustainable Chem. Eng.*, 2023, **11**, 343–352.
51 L. Tian, Y. Luo, K. Chu, D. Wu, J. Shi and Z. Liang, *Chem. Commun.*, 2019, **55**, 12976–12979.
52 L. Luo, X. Zhou, Y. Chen, F. Sun, L. Wang and Q. Tang, *Chem. Sci.*, 2025, DOI: **10.1039/D4SC07181F**.

© 2025 The Author(s). Published by the Royal Society of Chemistry